

Thermodynamics and statistical mechanics of the faceting of stepped Si(111)

Ellen D. Williams, R.J. Phaneuf, Jian Wei, N.C. Bartelt and T.L. Einstein

Department of Physics, University of Maryland, College Park, MD 20742-4111, USA

Received 15 February 1993; accepted for publication 6 May 1993

The thermodynamic formalism needed to analyze the faceting of surfaces is presented in a format readily applicable to experimental observations. Statistical mechanical predictions for the relationship of step and kink energies to the variation of the surface tension with orientation are reviewed and combined with the thermodynamic formalism to illustrate the physical mechanisms which can cause equilibrium faceting. The results show that faceting may be initiated by any process (such as reconstruction or chemical adsorption) which changes surface free energies by amounts comparable to the small ($\text{meV}/\text{\AA}$) energies of step–step interactions. The application of these methods is illustrated by analysis of our prior observations of faceting of stepped Si(111) surfaces, which is driven by the formation of the surface reconstruction. Using a nearest-neighbor square-lattice model with elastic step–step interactions to describe the surface, the only adjustable parameters are the kink energies and the step–step interaction energies. Given previous measurements of the magnitudes of the step–step interactions, we are able to reproduce quantitatively the three different phase diagrams which occur on different azimuths of vicinal Si(111). We extract from the fit to the data the variation in the difference of surface tension of the 7×7 and 1×1 -(111) surface with temperature, and values for the anisotropy in the step energy in the presence of the 7×7 reconstruction. We find that steps in the $[\bar{2}11]$ direction are at least $10 \text{ meV}/\text{\AA}$ more costly than steps on the unreconstructed surface, and steps in the $[2\bar{1}\bar{1}]$ direction are approximately $5 \text{ meV}/\text{\AA}$ less costly than steps on the unreconstructed surface. We discuss the requirements for determining absolute energies for steps and kinks given thermodynamic observations.

1. Introduction

As surface characterization improves, it is increasingly evident that large scale changes in surface structure can occur in processes such as chemical reaction and growth [1,2]. A particularly dramatic example of the lability of surfaces is the phenomenon of faceting, in which the surface rearranges into a hill-and-valley structure of increased surface area [3–10]. The basic thermodynamic principles governing faceting have been clear for a very long time [11], and there is an extensive literature of observations of faceting [12]. However, unambiguous identifications of equilibrium faceted surfaces, in sufficient detail for thermodynamic analyses to be applied, have appeared only recently [13–19]. Such observations provide an opportunity to obtain information about the anisotropy of the surface tension,

and about how the anisotropy is influenced by adsorption, reconstruction, and temperature. Furthermore, when such thermodynamic observations are combined with the results of direct imaging techniques, such as STM [20], LEEM [21], and REM [22], it becomes possible to understand faceting from an atomic point of view.

We will describe in the following the general thermodynamic and statistical mechanical formalism which can be used to analyze experimental measurements of faceting or to predict the conditions under which faceting may be expected to occur. As an example, we will apply this formalism to measurements of the faceting of vicinal Si(111) surfaces, unifying observations made by our group over the past several years [14,15,23–31]. The structure of one such faceted Si surface is illustrated in fig. 1 [32]. The faceting, which has increased the surface area by about one percent,

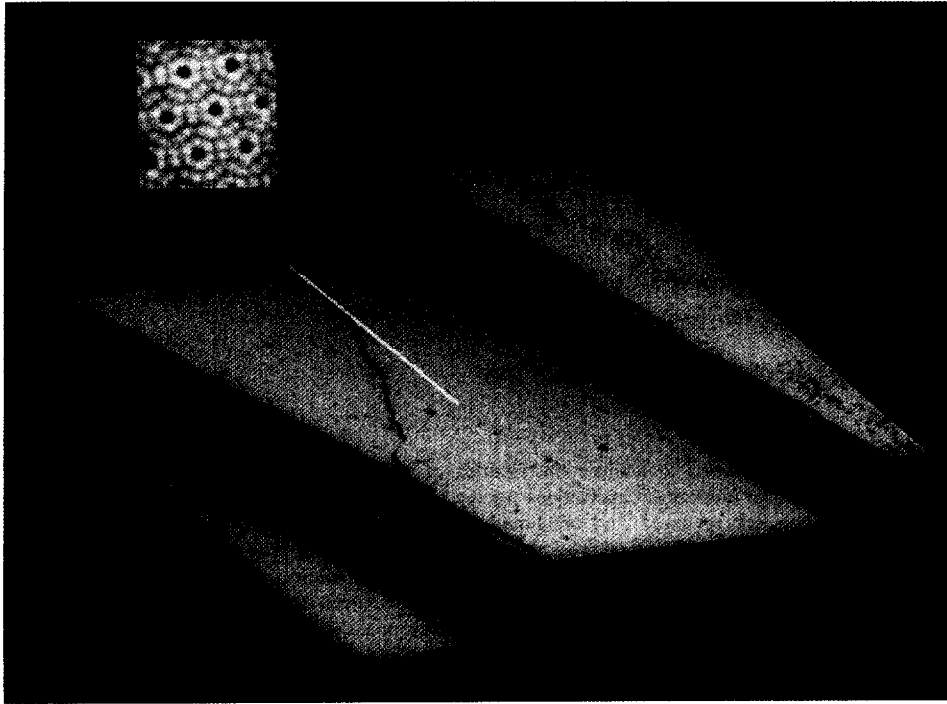


Fig. 1. A $2000 \text{ \AA} \times 2000 \text{ \AA}$ scanning tunneling microscope image of the phase separation of a vicinal Si surface. At high temperature this surface consisted of a uniform density of steps. (The net surface orientation is 4° from (111) towards $[\bar{2}11]$.) The two "phases" which appear at low temperature are the (7×7) reconstructed (111) facets and the unreconstructed step bunches. There are 10 steps in each step bunch. The surface normal of the step bunches is temperature dependent [14,15,58].

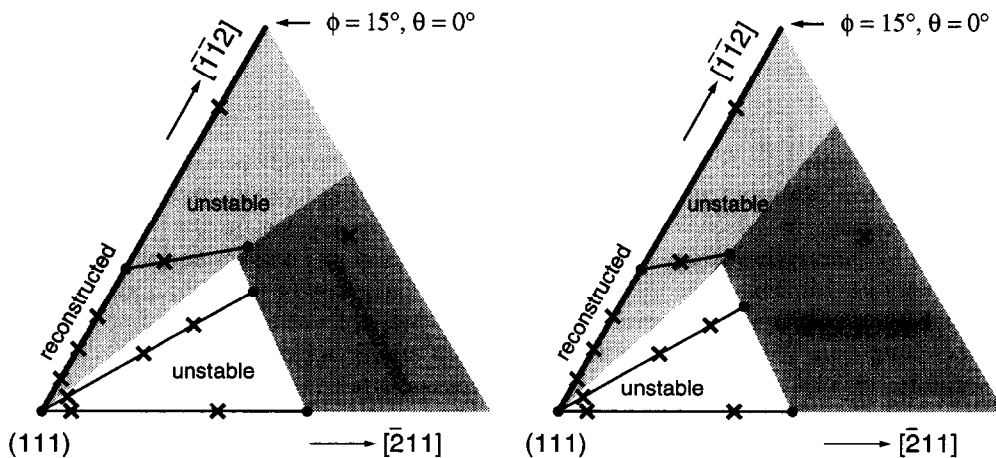


Fig. 2. Orientation phase diagrams of vicinal Si at 800°C (left panel) and 820°C (right panel), showing the form of the tie lines at various positions in density space. (Following eq. (8), this diagram is a polar plot of $\tan \phi$.) The \times 's mark the macroscopic orientations measured. The tie-bars terminate in the filled circles, which mark the observed boundaries of the coexistence regions. The shading indicates our estimated extrapolation of the phase boundaries to regions which have not been measured [31].

is driven by the formation of a surface reconstruction which lowers the surface tension of the low-index surface. Using LEED, we have characterized the orientational phase diagram for vicinal Si surfaces with a range of macroscopic azimuthal and polar angles with respect to the (111) orientation, as shown in fig. 2. These data tell us which surface orientations exist in phase equilibrium as a function of temperature. Combining these data with our additional observations of the step structure on the vicinal surfaces using STM allows us to interpret the phase equilibrium in terms of a simple model of step energetics. The adequacy of the chosen model is assessed by its quantitative applicability to a number of observations and by the physical significance of the energetic values deduced from the model. As we will show, it is possible to reconstruct a very complex set of phase transitions using a small set of adjustable parameters.

2. Thermodynamic methodology

Gibbs [33] recognized that surfaces will spontaneously rearrange to minimize their total surface tension, even if this involves an increase in surface area. Herring [11] quantified the conditions for a surface to break up into a hill-and-valley, or faceted, structure in terms of the orientational variation of the surface tension. For the case of a surface of an orientation \hat{n}_0 , where \hat{n} is a unit surface normal, to phase separate to two new orientations \hat{n}_a and \hat{n}_b as illustrated for the two-dimensional case in fig. 3, the requirements are simply that net orientation is conserved, and that total surface tension is reduced:

$$A_0 \hat{n}_0 = A_a \hat{n}_a + A_b \hat{n}_b, \quad (1)$$

$$A_0 \gamma(\hat{n}_0) > A_a \gamma(\hat{n}_a) + A_b \gamma(\hat{n}_b), \quad (2)$$

where γ is the surface tension and A_i is the area of the surface of orientation \hat{n}_i . One approach to evaluating the stability of surfaces based on these criteria is the construction of a Wulff plot to determine the equilibrium crystal shape [11,34–37]. Surfaces which do not exist on the equilibrium crystal shape are unstable with respect to faceting to orientations present on the equilibrium shape.

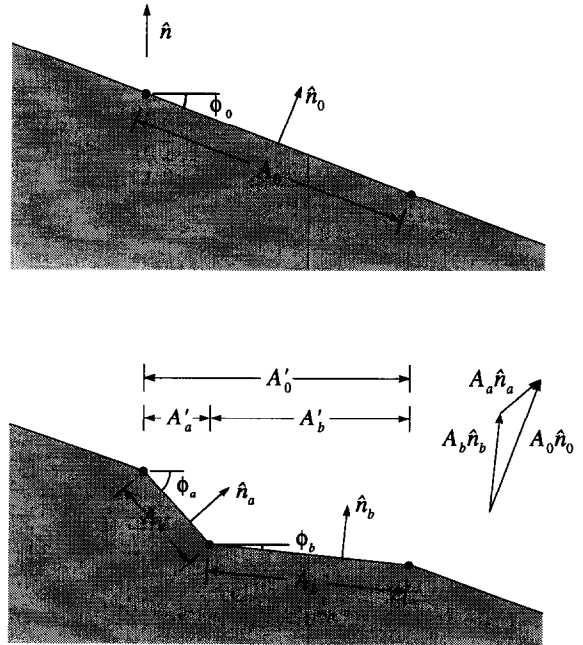


Fig. 3. A surface will be unstable with respect to faceting if the total surface tension decreases in going from the upper panel to the lower panel. Notice that the projected areas A'_i are additive (analogous to volume in fluids, and in contrast to the total areas). The requirement of conservation of macroscopic orientation, given by eq. (1), is illustrated in the insert.

Unfortunately, the relationship between the orientational variation of the surface tension and the surface stability is cumbersome to apply quantitatively. A more easily applied approach to evaluating the conditions for faceting is to define a free energy for which the standard convexity arguments familiar to phase separation in fluids apply [38–41]. To make this analogy with phase separation we need to define a “specific free energy” f , an extensive parameter A' (analogous to “volume”) related to the surface area, and a corresponding “density”, ρ . We will choose the definitions of these parameters such that the convexity requirement for phase separation in terms of these variables is:

$$A'_0 = A'_a + A'_b, \quad (3)$$

$$A'_0 f(\rho_0) > A'_a f(\rho_a) + A'_b f(\rho_b), \quad (4)$$

$$\frac{A'_b}{A'_a} = \frac{\rho_a - \rho_0}{\rho_0 - \rho_b}. \quad (5)$$

Geometric considerations illustrated in fig. 3 immediately show that the definitions of the extensive “area” parameter and the “specific surface free” energy which satisfy eqs. (3) and (4) are the projections of the true area and the surface tension into a reference plane of orientation \hat{n} ,

$$A'_i = A_i \hat{n}_i \cdot \hat{n}, \quad (6)$$

$$f_i = \frac{\gamma(\hat{n}_i)}{\hat{n}_i \cdot \hat{n}}. \quad (7)$$

We will refer to f as the reduced surface tension and A' as the projected area. Chernov noted that the appropriate thermodynamic density should be the step density $\rho = \tan \phi$ [39]. When we define the surface orientation in spherical coordinates by defining a polar angle ϕ , illustrated in fig. 3, and an azimuthal angle θ , we find by manipulating the vector components of eq. (1) that the step density is a vector, and that either of its two components can satisfy eq. (5):

$$\rho_x^i = \tan \phi_i \cos \theta_i, \quad (8a)$$

or

$$\rho_y^i = \tan \phi_i \sin \theta_i, \quad (8b)$$

if we choose the reference plane as a low index surface for which the polar angle $\phi_{\hat{n}}$ is zero (such that $\hat{n}_i \cdot \hat{n} = \cos \phi$, and eqs. (6) and (7) have correspondingly simple forms). We thus can apply the convexity requirement to orientational phase separation between two orientations \hat{n}_a and \hat{n}_b by considering the reduced surface tension as a function of the vector density defined by eq. (8) as illustrated in fig. 4. We can construct the tie-bars relating the phases in equilibrium according to the geometric requirement that the tie-bars be tangent to the reduced surface tension at the two points \hat{n}_a and \hat{n}_b . (This can be expressed equivalently as requirements on the equality of the intensive parameters conjugate to A' , ρ_x and ρ_y [42].)

As illustrated in fig. 5, the magnitude of thermodynamic density of eq. (8), $\rho = \sqrt{\rho_x^2 + \rho_y^2} = \tan \phi$, can be interpreted physically as the step density on a vicinal surface. The two components are the step density projected onto the high symmetry direction (x) and an orthogonal direction

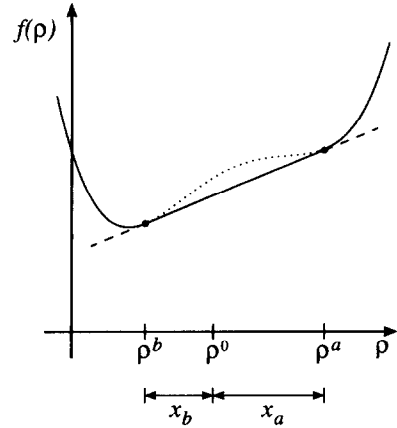


Fig. 4. Orientational phase separation occurs when a “hill-and-valley” structure has a lower total surface tension than a flat surface, as in eqs. (2) and (4). This translates into a convexity requirement on the “reduced surface tension” (which is analogous to a Helmholtz free energy) versus either component (eq. (8)) of the step density, $\hat{\rho}$. The figure illustrates a non-convex surface tension curve which would lead to faceting. The illustrated curve is schematic only: the form shown would occur physically only if there are attractive interactions between steps strong enough to overcome entropic and elastic interactions. The phase separation is indicated by the tie-bar connecting points a and b. For a macroscopic orientation $\hat{\rho}_0$ the relative areas of the orientations $\hat{\rho}_a$ and $\hat{\rho}_b$ are found from eq. (5), as illustrated in the figure with $x_a/x_b = (\rho_a - \rho_0)/(\rho_0 - \rho_b) = A'_b/A'_a$.

(y). The azimuthal angle θ in this description is the angle between the average direction of the step edge and the direction perpendicular to a high symmetry reference direction on the facet. It is thus physically related to the density of kinks on the step edge [43]. This physical interpretation of the density components becomes particularly useful in interpreting observed orientational phase diagrams in terms of atomic models of the surface, as discussed in section 3. Statistical mechanical descriptions of stepped surfaces use the step and kink densities as the fundamental units of the structure to predict how the surface tension varies with orientation in terms of model sets of energetic parameters. By comparison with these predictions, it is possible to extract information about the energetics of stepped surfaces from experimental observations of orientational phase separation. We will illustrate this process below for surfaces with orientations near a low-

index plane. The statistical mechanical description of the variation of the reduced surface tension with orientation which we will use is [35]:

$$f(\phi, \theta, T) = f^0(T) + \frac{\beta(\theta, T)}{h} |\tan \phi| + g(\theta, T) |\tan \phi|^3, \quad (9)$$

where $f^0(T) = f(0, 0, T)$ is the surface tension of the reference plane, $\beta(\theta, T)$ is the free energy cost per unit length of creating an isolated step, h is the step height, and $g(\theta, T) |\tan \phi|^3$ is the free energy cost per unit area due to step-step interactions. The variations of the step formation and step interaction terms with both temperature and azimuthal angle θ are governed by the kink energy ε . For temperatures well below the roughening transition of the low-index surface, specific functional forms for β and g can be derived for specific atomic models of the stepped surface,

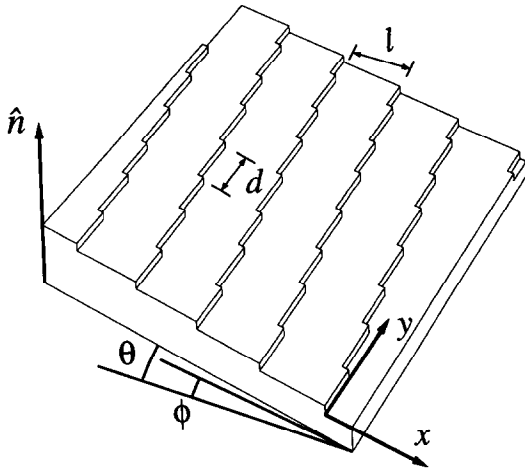


Fig. 5. A surface vicinal to a high index surface will be composed of a density of steps and kinks determined by the misorientation angles θ and ϕ . The number density of steps is $\tan \phi = \rho = h / \langle l \rangle$, where h = the step height and $\langle l \rangle$ = the distance between steps. When we define a reference direction in the reference surface for which the azimuthal angle θ equals zero, the number density of kinks is $\tan \theta = a_n / \langle d \rangle$, where a_n is the kink depth and $\langle d \rangle$ is the average distance between kinks. In thermal equilibrium there will be a distribution of step-step and kink-kink separations, leading to step wandering. Perfectly periodic spacings are shown in the figure simply for clarity.

and used for quantitative analysis of experimental observations as discussed in section 3.

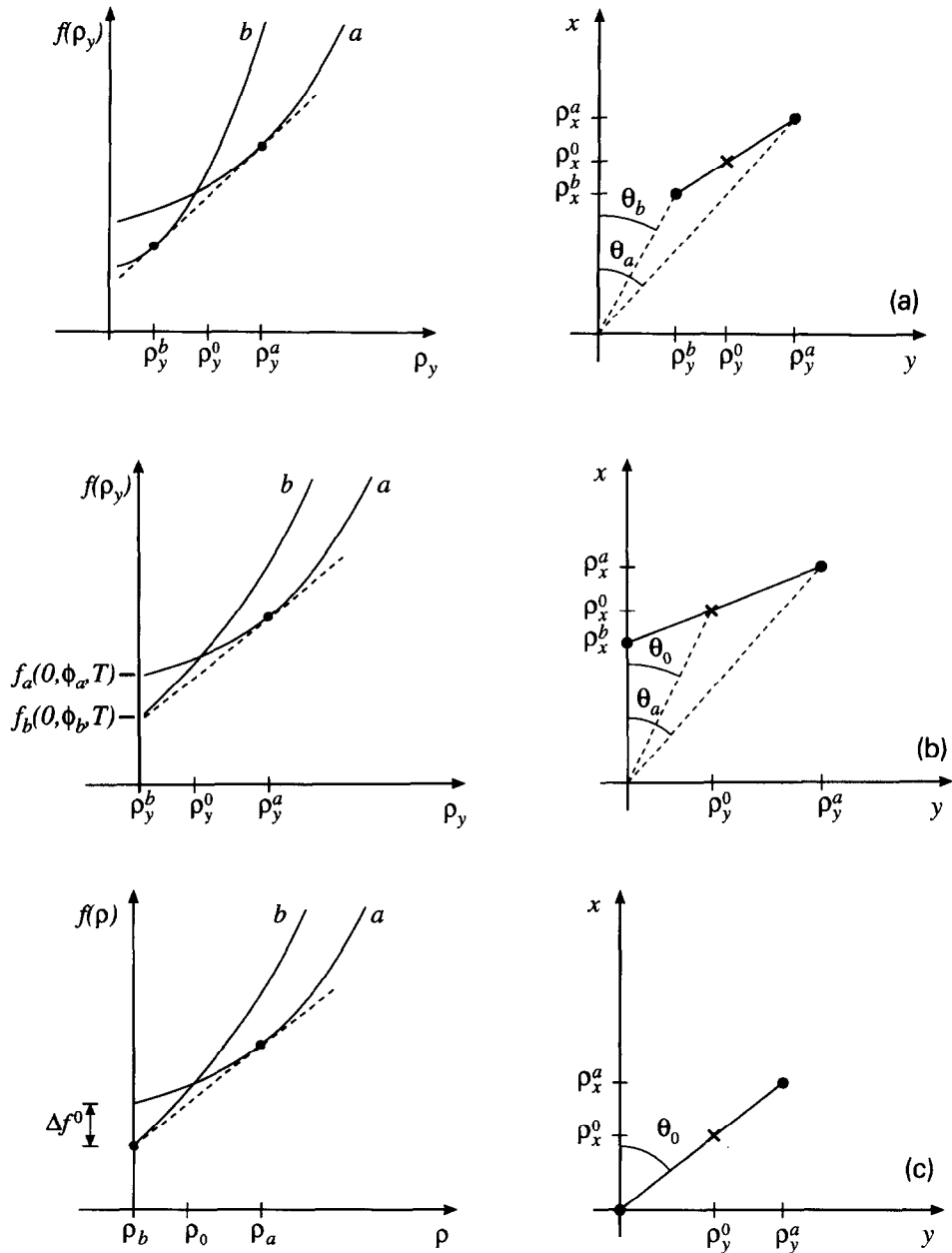
An orientational instability may arise from the intrinsic variation of the surface tension with orientation, as is illustrated in fig. 4. However, real vicinal surfaces are most often observed to be stable with respect to faceting [7,44], so we can expect that a monotonic variation of free energy with angle, such as described by eq. (9), will usually be appropriate for clean surfaces. In contrast, orientational instability (faceting) is frequently induced by chemical adsorption or by structural phase transitions. As proposed by Cahn [45], this can be understood by considering that the additional process completely alters the orientational variation of the reduced surface tension, resulting in intersecting curves as shown in fig. 6. In this case the phase separation occurs not only between different orientations, but also between different compositions (in the case of adsorption) or structures (in the case of phase transitions). In the following, we will present an analysis of the conditions governing phase separation in the case of such intersecting curves. In fig. 6, we illustrate three types of phase separation that might occur for a surface of arbitrary polar and azimuthal angle (ϕ_0, θ_0) near to a low index orientation $(\phi = 0)$. The three cases are: (1) separation to two arbitrary orientations, ϕ_a, θ_a and ϕ_b, θ_b for which the reduced surface tension is smoothly varying (differentiable); (2) separation between an arbitrary orientation ϕ_a, θ_a and an orientation $\phi_b, \theta_b = 0$ where there is a singularity in the reduced surface tension for $\theta_b = 0$; and (3) finally separation between an orientation $\phi_a, \theta_a = \theta_0$ and the orientation of the low index surface $\phi_b = 0$ when there is a cusp in the reduced surface tension for the low-index surface. The projection of the tie-bar into the $\tan \phi$ - θ plane for each of the three cases, and the variation of the reduced surface tension of the two phases with appropriate components of the step density are shown in fig. 6.

2.1. Case 1

In order to have a tie-bar between points a and b when the reduced surface tension has no

cusps, there must be a plane which is tangent to the two reduced surface tension curves at both points a and b. This requirement results in three equations which specify that the two components of the slope must individually be equal, and that

a plane of the overall slope actually intersects both points. If we define ρ_x and ρ_y axes, corresponding to $\theta = 0^\circ$ and 90° , respectively, as in fig. 6a, three equations determined by these conditions are, first, that the slopes (which can be



viewed as the orientational chemical potentials or “torques” [46]) at the two points are the same:

$$\left. \frac{\partial f_a(\theta_a, \phi_a)}{\partial \rho_x^a} \right|_{\rho_y^a} = \left. \frac{\partial f_b(\theta_b, \phi_b)}{\partial \rho_x^b} \right|_{\rho_y^b}, \quad (10a)$$

and

$$\left. \frac{\partial f_a(\theta_a, \phi_a)}{\partial \rho_y^a} \right|_{\rho_x^a} = \left. \frac{\partial f_b(\theta_b, \phi_b)}{\partial \rho_y^b} \right|_{\rho_x^b}, \quad (10b)$$

along with

$$\begin{aligned} f_b(\theta_b, \phi_b) = f_a(\theta_a, \phi_a) & \\ + (\rho_x^b - \rho_x^a) \left. \frac{\partial f_a(\theta_a, \phi_a)}{\partial \rho_x^a} \right|_{\rho_y^a} & \\ + (\rho_y^b - \rho_y^a) \left. \frac{\partial f_a(\theta_a, \phi_a)}{\partial \rho_y^a} \right|_{\rho_x^a}. & \quad (11) \end{aligned}$$

When we have a specific expression for the variation of the reduced surface tension with orientation, we can evaluate these expressions explicitly. Using eq. (9), and the formalism outlined in the appendix, allows us to obtain the relationships:

$$\begin{aligned} \left. \frac{\partial f_i}{\partial \rho_x} \right|_{\rho_y} = \frac{\beta_i}{h_i} \cos \theta_i + 3g_i \tan^2 \phi_i \cos \theta_i & \\ - \left(\frac{1}{h_i} \frac{\partial \beta_i}{\partial \tan \theta} + \frac{\partial g_i}{\partial \tan \theta} \tan^2 \phi_i \right) & \\ \times \left(\frac{\tan \theta_i}{\cos \theta_i} \right), & \quad (12) \end{aligned}$$

$$\begin{aligned} \left. \frac{\partial f_i}{\partial \rho_y} \right|_{\rho_x} = \frac{\beta_i}{h_i} \sin \theta_i + 3g_i \tan^2 \phi_i \sin \theta_i & \\ + \left(\frac{1}{h_i} \frac{\partial \beta_i}{\partial \tan \theta} + \frac{\partial g_i}{\partial \tan \theta} \tan^2 \phi_i \right) & \\ \times \left(\frac{1}{\cos \theta_i} \right). & \quad (13) \end{aligned}$$

Combining eqs. (10)–(13), with *no* assumptions about the forms of the parameters β and g , gives the general result:

$$\begin{aligned} f_a^0 - f_b^0 = 2g_a(\theta_a, T) |\tan \phi_a|^3 & \\ - 2g_b(\theta_b, T) |\tan \phi_b|^3, & \quad (14) \end{aligned}$$

where the difference in the surface tension of the two phases at $\phi = 0$ is $\Delta f^0(T) = f_a^0 - f_b^0$. This result shows that phase separation can occur for any process that changes the surface tension of the neighboring low-index surface by an amount comparable to the contribution of the step-interaction energy to the surface tension.

2.2. Case 2

In the second type of phase separation, illustrated in fig. 6b, we imagine that the reduced surface tension for one of the phases, f_b , has a knife-edge singularity along the high symmetry direction, $\theta_b = 0$. In this case we cannot require that the y -component of the tie-bar be tangent to

Fig. 6. A change in surface composition (e.g. due to adsorption or segregation) or structure (e.g. due to a phase transition) can change the variation of the surface tension with orientation. If the curve for a “perturbed” surface, labeled b, intersects that of the “unperturbed” surface, labeled a, then the convexity requirement illustrated in fig. 4. will lead to orientational phase separation. The new surface orientations exposed will have the vector densities $\hat{\rho}_a$ and $\hat{\rho}_b$. The surfaces of orientation $\hat{\rho}_a$ will have the composition or structure of the “unperturbed” phase, and those of orientation $\hat{\rho}_b$ will have the composition or structure of the “perturbed” phase. The figure illustrates schematically how intersecting free energy curves lead to faceting. In the left hand column are shown the variation of the projected surface tension with one component of the vector density, eq. (8). Because the intersecting curves lead to a projected surface tension curve which is not convex, there is a region of unstable orientations, leading to step rearrangement to form facets. The corresponding projections of the phase diagrams into the θ - ϕ plane are shown in the right hand column. The three general types of tie lines one might expect from the faceting of vicinal surfaces: (a) No cusps are involved. The convexity requirement is applicable to the variation in reduced surface tension with both components ρ_x and ρ_y of the step density. (The variation with ρ_x is shown.) Thus eqs. (10)–(14) determine the misorientation angles of the two phases. (b) If there is a knife-edge cusp along a high symmetry direction, one of the ends of the tie line can intersect the cusp, removing one of the tangency requirement, and replacing it with the inequality of eq. (15). (c) If there is a deep cusp in the surface tension at the low-index surface ($\phi = 0$), one of the ends of the tie line can intersect the cusp, leading to phase separation in the polar angle, leaving the azimuthal angle fixed. In this case the convexity requirement on the free energy is expressed in terms of the magnitude of the step density, rather than its vector components, as in eq. (16).

the reduced surface tension curve at $\theta_b = 0$, and we lose the requirement of eq. (10b). However, for phase separation to $\theta_b = 0$ to occur, the slope of the reduced surface tension curve as it approaches $\theta_b = 0$ must be greater than the slope of the tie-line. Thus eq. (10b) can be replaced by an inequality corresponding to

$$\left. \frac{\partial f_a}{\partial \rho_y^a} \right|_{\rho_x^a} < \left. \frac{\partial f_b}{\partial \rho_y^b} \right|_{\rho_x^b; \rho_y^b \rightarrow 0}. \quad (15)$$

Eq. (10a) remains valid. Because the slope of the tie-bar must still match the tangent of free energy curve for phase a, the form of eq. (14), which describes the difference in the surface tension between the two phases, is also unchanged. The derivatives of the reduced surface tension of phase b, eqs. (12) and (13), are simplified in form as $\theta_b = 0$.

2.3. Case 3

In the final type of phase separation, illustrated in fig. 6c, we imagine that the reduced surface tension for one phase has a cusp-like singularity at $\phi_b = 0$. In this case we have no information about the behavior of the system with azimuthal angle, so we are reduced to two independent equations describing the system, rather than three. Furthermore, because of the cusp, the requirement on the slope becomes an inequality which can be written most usefully as:

$$\left. \frac{\partial f_a}{\partial \tan \phi_a} \right|_{\theta_a} < \left. \frac{\partial f_b}{\partial \tan \phi_b} \right|_{\theta_b = \theta_a, \phi_b \rightarrow 0}. \quad (16)$$

Eq. (14) still remains valid because of the requirement that the slope of the tie-bar matches the tangent to the free energy of curve a, but it is simpler in form since $\phi_b = 0$:

$$\Delta f^0 = f_a^0 - f_b^0 = 2g_a(\theta_a, T) |\tan \phi_a|^3. \quad (17)$$

3. Statistical mechanical methodology

Extracting specific values for atomic energies from thermodynamic observations is always

fraught with problems of uniqueness. For the particular case of stepped surfaces, the thermodynamic behavior is completely defined by the tendency of steps to wander, with the result that one can obtain unique information about the step “stiffness” (defined below) which characterizes step wandering [43]. To proceed from a value of the stiffness to a determination of the characteristic energies of the system, one must choose a reasonable microscopic model using either assumptions or additional information available about the system. It is sensible to begin this process by invoking the simplest possible microscopic model that can produce the phenomena of interest. One then uses the observations to fit the microscopic energies of this model. In evaluating how well the energies thus determined describe the true physical energies of the system, consistency of all observations with the model is necessary of course, but not sufficient. Our goal in the analysis of the Si(111) data will be to find the minimal parameter set sufficient to describe our observations, and to use it to extract estimates for the values of the step and kink energies. We will then discuss the extent to which these model-dependent values can be used to understand the physical step and kink energies. In the course of the analysis, we will also evaluate the general questions of what physical factors are important in determining faceting, and what the important energy scales are.

In this spirit, we present specific predictions for the parameters of eq. (9) in terms of a nearest-neighbor square lattice model, with the addition of a long-range repulsion between steps. There are three energetic parameters in this model: the energy cost $\beta(0, 0)$ per unit length of creating a step at $T = 0$ in the high symmetry ($\theta = 0$) direction, the energy ε of creating a single kink of depth a_n (depth is defined normal to the step edge), and the magnitude of the step–step repulsions. More complex models, including kink corner energies [43,47], non-linear variation of kink energy with kink size [43], kink–kink interactions [48], honeycomb symmetry, and different forms for the step–step interactions [49–51] can be considered with correspondingly more complex forms of the equations below.

The leading term in the expression for the surface tension as a function of orientation, eq. (9), is the linear variation of the surface tension with step density. The coefficient of this term, $\beta(\theta, T)$, is the free energy per unit length of an isolated step. For arbitrary temperatures, the step free energy can be calculated using forms for the interface energy for the Ising model with both isotropic [52] and anisotropic [41] near-neighbor interactions. The use of isotropic interactions is equivalent to assuming a square lattice in which the zero-temperature energy cost of steps equals the kink energy per unit length, $\beta(0, 0) = \varepsilon/a_k$, where a_k is the length of the kink edge ($a_k \geq a_n$, with the equality occurring when the kink is perpendicular to the step edge). The square-lattice model is a reasonable zeroth-order approach for the high-symmetry Si(111) surface which will be discussed in section 4. However, for a lower symmetry surface, such as Si(100) [47,53], the kinks and steps have different bonding configurations, and thus a rectangular lattice model, for which one would use the anisotropic calculation, would be more appropriate. The results of the Ising model analogy give the step free energy for steps

in the high symmetry direction, $\theta = 0$, as

$$\beta(0, T) \approx \beta(0, 0) - \frac{kT}{a_p} \ln \left(\coth \frac{\varepsilon}{2kT} \right), \quad (18a)$$

where a_p is the minimum separation between kinks along the step edge. At low temperatures, this equation can be approximated by [31]:

$$\beta(0, T) \approx \beta(0, 0) - \frac{2kT}{a_p} \exp \left(\frac{-\varepsilon}{kT} \right). \quad (18b)$$

Analytical expressions for the variation of $\beta(\theta, T)$ with $\tan \theta$ for all temperatures less than the Ising critical temperature ($kT_c \approx 1.13\varepsilon$) can be obtained for the symmetrical case with the substitution of $\varepsilon = 2J$ in the formulas given in ref. [52], and for the anisotropic case with the substitutions, $\beta(0, 0) = 2J_y/a_p$ and $\varepsilon = 2J_x$ in ref. [54]. The full isotropic formula, which we use in section 4 for analyzing the experimental observations on Si(111), is:

$$\begin{aligned} \frac{a_p}{kT} \beta(\theta, T) = & |\cos \theta| \sinh^{-1} [\alpha(\theta) |\cos \theta|] \\ & + |\sin \theta| \sinh^{-1} [\alpha(\theta) |\sin \theta|], \end{aligned} \quad (19a)$$

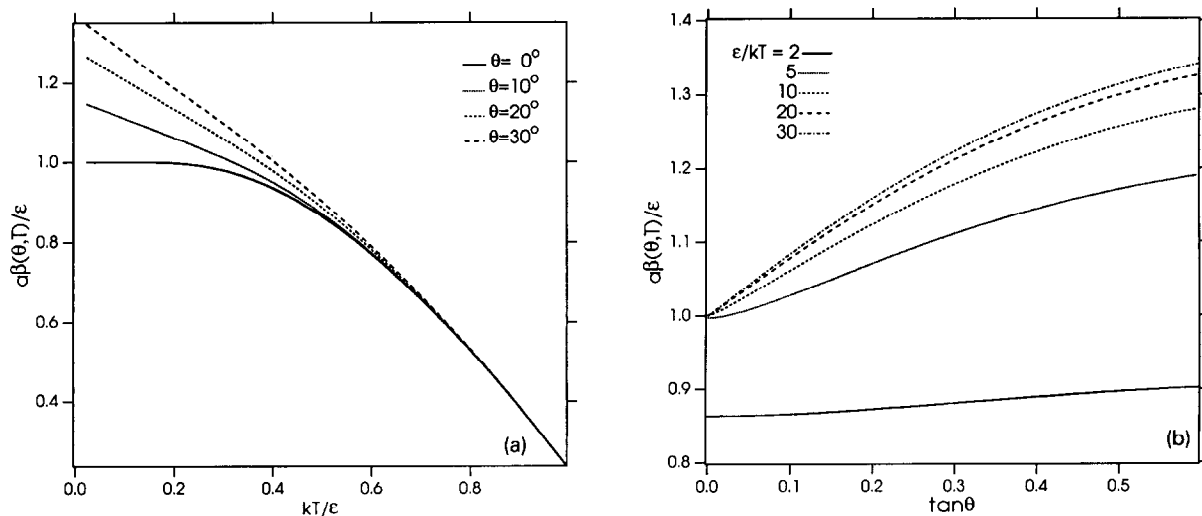


Fig. 7. The free energy per unit length of a step $\beta(\theta, T)$ calculated for the square nearest-neighbor lattice model, using eq. (19). (a) Step energy versus temperature for several values of the net azimuthal angle. (b) Step energy versus tangent of the azimuthal angle for several values of the temperature. When the temperature is high relative to the kink energy ε , step wandering lowers the step free energy and makes it relatively isotropic. When the temperature is low, there is a significant energy cost to changing the orientation away from the high-symmetry direction.

where

$$\alpha(\theta) = \frac{2}{c} \left[\frac{1 - c^2}{1 + (\sin^2 2\theta + c^2 \cos^2 2\theta)^{1/2}} \right]^{1/2}, \quad (19b)$$

and

$$c = \frac{2 \sinh(\varepsilon/kT)}{\cosh^2(\varepsilon/kT)}. \quad (19c)$$

At $T = 0$, the step energy reduces to

$$\beta(\theta, 0) = \beta(0, 0) \cos \theta + \frac{\varepsilon}{a_p} |\sin \theta|, \quad (20)$$

where $\beta(0, 0) = \varepsilon/a_k$ in the isotropic case. The form of eq. (20) indicates a cusp in the step energy at $\theta = 0$. At any non-zero temperature the entropy contribution due to the random distribution of kink sites removes the cusp at $\theta = 0$. However, differentiation of eq. (19) with respect to θ shows that the transition from zero slope to a large positive slope occurs at extremely small values of θ for values of $\varepsilon/kT \geq 5$. Thus, behavior which appears experimentally very much like the knife edge singularity discussed in section 2.2 may be observed for large kink energies or low temperatures. The variation of the step free energy with temperature and with kink density, $\tan \theta$, calculated using eq. (19), is shown in fig. 7. The slopes of the β - $\tan \theta$ curves, which are important in evaluating eqs. (12) and (13), are calculated numerically for the analysis of section 4.

The final term in the expression for the step free energy is due to the interactions between steps. The form and magnitude of this term are determined by step wandering due to thermal excitation of kinks, as well as any energetic interactions between the steps such as elastic or dipolar repulsions. This wandering can be described by the "step diffusivity", $b^2(\theta, T)$, which can be calculated as the mean-square displacement of the step edge when there are no kink-kink interactions [43]. Closed forms for the step diffusivity can be calculated for the case where no overhanging kinks exist, the unrestricted TSK (terrace-step-kink) model. For steps along the high-sym-

metry direction $\theta = 0$, these equations are reasonably applied for $kT < \varepsilon$, the kink energy. Within this approximation, the expression for the step diffusivity is easily shown to be [43]:

$$\frac{b^2(T)}{a_n^2} = \frac{2z_0}{(1 - z_0)^2}, \quad (21)$$

where

$$z_0 = \exp(-\varepsilon/kT).$$

For steps with a misorientation angle θ , there is an intrinsic kink density proportional to $\tan \theta$. Within the TSK approximation, the derivation of the step diffusivity including the dependence on azimuthal angle yields [43]

$$\frac{b^2(\theta, T)}{a_n^2} = \tan^2 \theta + \frac{h + C\sqrt{(1 + \tan^2 \theta)D - C^2 \tan^2 \theta}}{C^2 - D}, \quad (22)$$

where

$$D = 4z_0^2 + (C^2 + C) \tan^2 \theta,$$

and

$$C = 1 + z_0^2.$$

This equation is valid only for small values of θ , as overhangs quickly become important for $\theta \geq 5^\circ$. In order to calculate the diffusivity at arbitrary angles, one can use its relationship to another important quantity, the step-edge "stiffness" $\tilde{\beta}$ via [55,56]

$$\tilde{\beta}(\theta, T) = \frac{kT a_n}{b^2(\theta, T) \cos^3 \theta}. \quad (23)$$

The step edge stiffness can in turn be calculated from its relationship to the step free energy $\beta(\theta, T)$:

$$\tilde{\beta}(\theta, T) = \beta(\theta, T) + \frac{\partial^2 \beta(\theta, T)}{\partial \theta^2}. \quad (24)$$

The step edge stiffness diverges at $T \rightarrow 0$ for high-symmetry ($\theta = 0$) steps, which makes direct calculation of the diffusivity using eqs. (21) or (22) useful at low temperature or small angle.

The variation of the step diffusivity with angle, calculated using eqs. (19), (23) and (24), is shown in fig. 8.

Once an expression for the step stiffness or diffusivity is obtained, it can be used to evaluate the step-step interaction term, $g(\theta, T)$ in eq. (9). The general form for this term, valid when the step diffusivity is much smaller than the square of the average step separation [35,57], is

$$g(\theta, T) = \frac{\pi^2 k T b^2(\theta, T)}{48 a_p h^3} \times \left\{ 1 + \left[1 + \frac{8 A a_p}{k T b^2(\theta, T)} \right]^{1/2} \right\}^2 \quad (25a)$$

for step-step interactions of the form $U(x) = A/x^2$. The temperature dependence of this term depends on two characteristic energies, the kink energy and the interaction energy. The variation of the step interaction term with kink density, $\tan\theta$, is shown in fig. 9 for a specific ratio of the step interaction strength A to the kink energy ϵ . A useful limiting form for the step-step interactions for $A = 0$ is,

$$g(\theta, T) = \frac{\pi^2 k T b^2(\theta, T)}{12 a_p h^3}. \quad (25b)$$

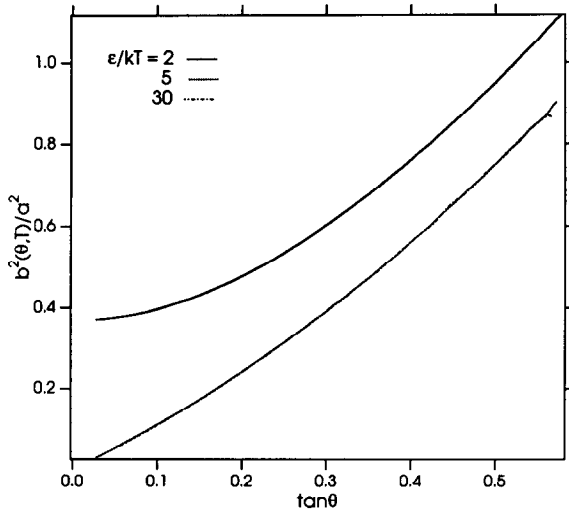


Fig. 8. The step diffusivity $b^2(\theta, T)$ as a function of azimuthal angle, calculated from eqs. (23) and (24), using the values of the step free energies shown in fig. 7. The diffusivity increases with kink density and with temperature. By $\epsilon/kT = 5$, b^2 has reached its $T = 0$ limit.

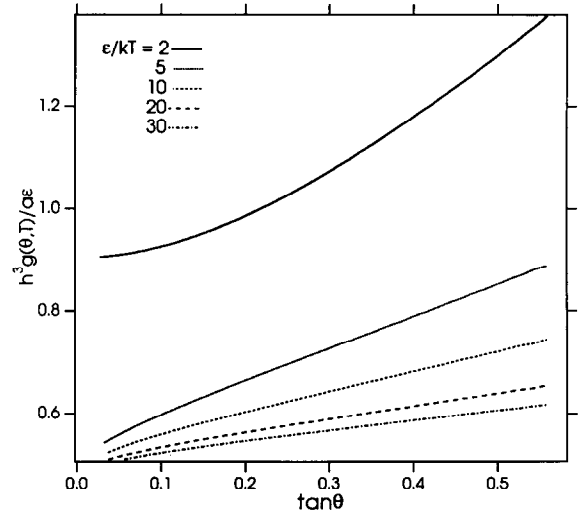


Fig. 9. The contribution of step interactions to the reduced surface tension coefficient, $g(\theta, T)$, as a function of the azimuthal angle, calculated using eq. (25) with the values of the diffusivity shown in fig. 8. The strength of the step-step interaction used in the calculation is $A/a_p \epsilon = 0.22$. The magnitude of the interaction coefficient increases with increasing step wandering.

For low temperature and misorientation angle, the step diffusivity goes to zero and another simple form results:

$$g(\theta \rightarrow 0, T \rightarrow 0) = \frac{\pi^2 A}{6 h^3}. \quad (25c)$$

Finally, we will also need to consider the variation of the step interaction term $g(\theta, T)$ with $\tan\theta$. If all the θ -variation enters through $b^2(\theta, T)$ (in other words, if the step-step interaction strength A is independent of angle, as it should be for elastic interactions on surfaces with three-fold or higher symmetry), we find easily that $\partial g / \partial \tan\theta \rightarrow 0$ at $\theta = 0$. The values of the derivative at non-zero angles were calculated numerically from eq. (25a) for the analysis of section 4.

4. Analysis

We will apply the analysis developed above to the orientational phase diagram of Si(111) illustrated in fig. 2 [17]. In particular, we will concentrate on the orientational phase separations that

Table 1

The measured values of the angles at the phase boundaries illustrated in fig. 2 are listed below for a few selected temperatures, which will be used in the following for quantitative analysis

T (°C)	Reference direction					
	$[\bar{2}11]$		$[\bar{1}\bar{1}2]$			
	ϕ_a	ϕ_b	ϕ_a	θ_a	ϕ_b	θ_b
≥ 845	ϕ°	–	6.7°	8.6°	–	–
820	8°	0°	8°	17°	5.7°	0°
800	10°	0°	9°	21°	5.7°	0°
770	12°	0°	11°	26°	5.7°	0°
645	18°	0°				
RT	20°	0°	$\sim 14^\circ$	$\sim 40^\circ$	5.7°	0°

Graphical presentations of the complete phase boundaries with respect to temperature have been published previously [14,15,17,27,68]. In addition, previous observations have shown that for orientations exactly on the $[\bar{1}\bar{1}2]$ axis, faceting does not occur. Along this azimuth, the transition temperature at which both the surface reconstruction and the step height changes is independent of the polar angle [28]. The subscript a refers to the high-temperature “ 1×1 ” phase, and the subscript b refers to the low-temperature 7×7 phase.

we have previously characterized using LEED [14,15,17], which appear as tie-bars in fig. 2. Numerical values for the measured boundaries of the phase diagrams are listed for a few temperatures in table 1. As we have shown previously, these phase separations occur in reversible phase transitions, which are driven by the formation of the 7×7 reconstruction of the (111) surface. The faceted surfaces represent phase coexistence between two different orientations, on one of which the 7×7 reconstruction exists, and on the other of which there is the structure of the high-temperature “ 1×1 ” phase [58]. Thus, in order to analyze these transitions according to the methodology of section 2, we must have information about the high-temperature, unreconstructed phase. We are fortunate that lovely studies of step behavior on vicinal Si(111) surfaces at high temperature have been performed using REM [22,59,60]. Alfonso et al. [60] have made direct observations of the wandering of isolated steps. Their results show that at 900°C , the step edge stiffness is $6.8 \times 10^{-2} \text{ eV}/\text{\AA}$. Using eq. (23), we can use this result to estimate the step diffusivity

$b^2(900^\circ\text{C}) \approx 5.7 \text{ \AA}^2$, and thus from eq. (21) the kink energy $\epsilon \approx 0.18 \text{ eV}$ for the high-temperature phase [61]. This value of the kink energy is consistent with their observation that sublimation pits are roughly circular at 900°C , as calculations of the two-dimensional crystal shape within the isotropic Ising model show that the shape is close to circular to temperatures as low as $kT = 0.4\epsilon$ [54]. Alfonso et al. [60] have also measured the distributions of step–step separations for a large range of step densities, and have shown that the width of the step distribution is linear in the average separation with a slope between 0.29 and 0.34. Analysis of their results gives the step–step interaction energy $U_1 = A_1/l^2$, where $A_1 \approx 0.12\text{--}0.22 \text{ eV \AA}$ and l is the step–step spacing [62,63].

For analyzing the phase separations of fig. 2, we will also make use of the extensive body of existing information concerning the 7×7 reconstruction which is present at low temperature. LEEM studies of the formation of the 7×7 phase transition have shown that the reconstruction nucleates differently on steps misoriented toward the $[\bar{2}11]$ and the $[2\bar{1}\bar{1}]$ directions [64]. This behavior is consistent with the crystallographic anisotropy of the phase diagram of fig. 2. The anisotropy is also consistent with REM observations of etching spirals at 800°C , from which the step free energy in the $[2\bar{1}\bar{1}]$ was estimated to be 1.2–1.25 times lower than that in the $[\bar{2}11]$ direction [59]. It is also consistent with observations of the near-triangular shape of islands of Si grown on Si(111) [65]. Recent high-temperature LEEM [29,66] and STM [67] measurements have shown that the thermal motion of the step edge slows to unobservability as soon as the 7×7 reconstruction is complete. This suggests that all step rearrangements that occur below the 7×7 transition temperature (see fig. 2) must take place by motion of steps in the 1×1 phase. We have previously used STM to characterize step and kink distributions below the 7×7 transition temperature on surfaces misoriented along the $[2\bar{1}\bar{1}]$ direction. From those studies, we showed that (1) the terraces and kinks are quantized in the 7×7 unit cell [25], (2) there are no thermally excited 7×7 kinks on the steps (which we assume were equilibrated at about 800°C [63,67]), and (3) the step distribution is

consistent with a step-step interaction energy $U_7 = A_7/l^2$, where $A_7 \approx 0.4 \pm 0.1$ eV Å [63].

4.1. Phase separation along $[\bar{2}11]$ and $[1\bar{1}0]$

From LEED and HRLEED measurement of the temperature dependence of the orientational phase diagram, we have shown that the phase separation along these azimuths was between $\phi \leq 0.2^\circ$ for the 7×7 phase and $\phi > \phi_0$, the macroscopic polar angle, for the 1×1 phase. Measurements of the phase separation using X-ray diffraction [68] and RHEED [69] have also been made. These results suggest that phase separation occurs to a cusp in the surface tension of the 7×7 phase at $\phi = 0^\circ$. STM images of the facets [70–73], as shown in fig. 1 [32], confirm this hypothesis by showing that there is in fact no step density on the 7×7 facets. We can therefore treat this phase separation as an example of a case 3 phase transition, as discussed in section 2, with the 7×7 phase corresponding to orientation \hat{n}_b where $\phi = 0$, and the 1×1 phase corresponding to orientation \hat{n}_a . We thus should be able to obtain one equality, and one inequality among the parameters governing the surface tensions of the two phases. Given the value of the step-step interaction in the 1×1 phase, and the value of $\tan(\phi_a(T))$ from the phase diagram, we obtain the equality by using eq. (17) to determine the variation in the difference in the surface tension of the two phases $\Delta f^0(T)$ in the (111) plane with temperature. The numerical results are listed in table 2. The difference is very small: even 200°C below the transition, where ϕ_a is approximately 18° , the surface tension of the 7×7 phase is only approximately 1 meV/Å² smaller than that of the 1×1 phase. The value of the change in surface tension is reasonable on thermodynamic grounds: the derivative of the surface tension with respect to temperature is a specific entropy. One expects that the difference in entropy of two phases near a thermally driven first order transition to be on the order of k_B per atom. A change in γ of about 1 meV/Å² over a temperature range of 200 K corresponds to a difference of entropy (which is proportional to a latent heat [24]) of $0.6 k_B$ per surface atom. The general significance of the

Table 2
Energy values for steps on the $[\bar{2}11]$ azimuth

T (°C)	$g_a(0, T)$ (meV/Å ²)	$\Delta f^0(T)$ (meV/Å ²)	$\beta_b - \beta_a$ (meV/Å) (lower limit)	$\beta_a(0, T)$ (meV/Å) (from eq. (19))
845	15 ± 5	0	–	39 ± 7
820	14 ± 5	0.1 ± 0.03	3 ± 1	40 ± 7
800	14 ± 5	0.2 ± 0.05	4 ± 2	40 ± 7
770	14 ± 5	0.3 ± 0.1	6 ± 2	41 ± 7
645	12 ± 4	0.8 ± 0.3	12 ± 4	43 ± 7

The subscript a refers to the high temperature “ 1×1 ” phase, and the subscript b refers to the low-temperature 7×7 phase. The values $\varepsilon \approx 0.18 \pm 0.02$ eV and $A = 0.15 \pm 0.05$ eV Å were used in eqs. (22) and (25) to obtain the step-interaction prefactor, $g(0, T)$, and thus using the values of the phase boundary from table 1, the difference in the surface tension $\Delta f^0(T)$ of the 1×1 and 7×7 phases from eq. (14). The lower limit on the difference in the step free energies, was calculated from eq. (26). The absolute value of the step energy in the 1×1 phase, $\beta_a(0, T)$, was calculated using eq. (19) with a kink energy $\varepsilon = 0.18 \pm 0.02$ eV. The uncertainties listed in the table reflect the error bars on the parameters: the effect of experimental uncertainty in the phase diagram is reflected in the limited number of significant figures in the reported values.

small calculated value is the fact that changes in the surface tension of such small magnitude are sufficient to cause faceting of the surface. This is a direct result of eq. (17), which relates the difference in surface tension to the difference in the step interaction terms. The magnitude of the step interactions on Si(111) is consistent with the value expected if the interactions are mediated by the surface stress [63,74,75]. Since the surface stress is comparable in magnitude on most materials, and is likely to be the dominant effect in step interactions, the magnitude of the change in surface tension needed to allow faceting should also be comparable for any surface.

From the inequalities of eqs. (15) and (16), we can obtain additional limiting information about the differences of the step and kink energies in the two phases. We had speculated previously that the phase separation was driven by an increase in the step-formation free energy in the presence of the 7×7 reconstruction [14,15,24,27]. The physical interpretation is that an unfavorable step energy in the 7×7 phase causes the steps to

segregate into bunches which maintain the 1×1 reconstruction, leaving large unstepped regions of 7×7 structure. Such segregation is, of course opposed by the increased step interactions caused by the smaller step-step separations in the 1×1 phase. We can now quantify this interpretation by using eq. (16) to obtain:

$$\beta_b(0, T) - \beta_a(0, T) > 3g_a(0, T)h_a \tan^2 \phi_a, \quad (26)$$

where we have assumed that the step heights are the same in both phases, $h_a = h_b$. From eq. (26), we now confirm the qualitative interpretation, and determine that the minimum magnitude of the difference required to cause faceting is set by the strength of the step-step interactions. We can use eq. (25a) to obtain the value of $g_a(0, T)$ using the kink energy of $\varepsilon = 0.18$ eV. In order to obtain a feeling for the effect of statistical uncertainty on the value of the kink energy, a 10% uncertainty is assigned to the value of the kink energy in the calculation. The result is shown in table 2. We obtain the most stringent inequality by using a point on the phase diagram with the largest change in angle. Thus, using a temperature 200°C below the transition, we find that the lower limit on the difference in step free energies required to cause faceting can be small, $\Delta\beta(T) \geq 12$ meV/Å. As noted above, the small magnitude of this value is determined by the step-step interactions, and thus is a general result with significance for any process which changes the step energies. If we use eq. (19), with $\varepsilon = 0.18$ eV, to compute the value of the step free energy in the 1×1 phase, $\beta_a(0, T)$ as shown in the last column of table 2, we can then estimate the absolute energy of the $[\bar{2}11]$ step edge in the 7×7 phase to be $\beta_b(0, T) \geq 55$ meV/Å, or 1.5 eV/ 7×7 unit cell edge. In the isotropic model for step/kink energies, this number would also give the kink energy in the 7×7 phase of approximately 1.5 eV, corresponding to $\varepsilon/kT \approx 15$ at the transition temperature.

4.2. Phase separation along $[\bar{2}\bar{1}\bar{1}] \pm \theta$

The behavior of Si(111) vicinal surfaces along the $[\bar{2}\bar{1}\bar{1}]$ azimuth is completely different from that along the $[\bar{2}11]$ azimuth [28,76]. Surfaces

exactly on the $[\bar{2}\bar{1}\bar{1}]$ azimuth are orientationally stable, and the reconstructive transition temperature is independent of the angle of miscut. Upon cooling through the phase transition temperature, the surfaces maintain the original polar angle, and the step structure changes to a mixture of single- and triple-height steps, with the fraction of triples increasing with increasing polar angle. We have determined that the mixtures occur due to a competition between the step-step repulsion energy and a small energy cost for forming a triple-height step from three single-height steps, $\Delta E = \beta_t(T=0) - 3\beta_s(T=0) \approx 0.1$ meV/Å [63,75,77]. However, surfaces misoriented by an azimuthal miscut with respect to the $[\bar{2}\bar{1}\bar{1}]$ phase separate to a finite polar angle on the $[\bar{2}\bar{1}\bar{1}]$ azimuth, and to another orientation with larger polar and azimuthal angles, as illustrated in fig. 2 and table 1. On the basis of the LEED and STM data, we postulate that the variation of reduced surface tension of the 7×7 phase with azimuthal angle θ is close to a knife-edge singularity along the $[\bar{2}\bar{1}\bar{1}]$ azimuth. This is equivalent to assuming that the energy cost for kinks in the 7×7 phase is large, so that eq. (20) is a reasonable approximation to the variation of step energy with azimuth. The large kink energy would then drive the orientational phase separation by making expulsion of the kinks to a 1×1 surface of larger azimuthal miscut energetically favorable. Under this approximation, this phase separation can be described by the equations of case 2 (section 2.2), discussed in section 2. Thus, we are able to specify the parameters governing the phase separation with two equalities and one inequality. An interesting aspect of the observed phase separation is the fact that the polar angle of the 7×7 phase remains fixed as both the polar and azimuthal angles of the 1×1 phase change dramatically. As we will show below, this result is a natural consequence of the geometry of the transition.

The first equality is eq. (14), which gives us the difference in surface tension between the (111) facet with 1×1 and with 7×7 reconstruction. We have determined this value above from the data for the polar phase separation. Here we will determine it independently from the data for the azimuthal phase separation. In this case, the dif-

ference is determined by the strength of the step–step repulsions in the two phases, which is affected by the non-zero azimuthal angle in the 1×1 phase. If we assume that the kink energy in the 7×7 phase is much larger than the thermal energy, then we can use eq. (25c) to estimate $g_b \approx \pi^2 A_b / 6h^3 = 0.022 \pm 0.006 \text{ eV}/\text{\AA}^2$ for single-height steps, and one third of this value, $g_b \approx 0.007 \pm 0.002 \text{ eV}/\text{\AA}^2$ for triple-height steps. The value of the step interaction term can be calculated using eq. (25a) with the estimated kink energy of the 1×1 phase, $\epsilon = 0.18 \pm 0.02 \text{ eV}$ [78]. The values are listed in table 3, along with the calculated value of the difference in the surface tension. The values of $\Delta f^0(T)$ are in excellent agreement with those calculated from the data on phase separation in the $[\bar{2}11]$ direction, indicating internal consistency of the model.

The equality of one slope of the free energy curves (eqs. (10a) and (12)) allows us to obtain information about the differences of the step and kink energies between the two phases. We have speculated previously that this azimuthal phase separation occurs due to a large energy cost for kinks in the presence of the 7×7 reconstruction [17]. Thus at the transition temperature there is a strong driving force for steps to be oriented along the high-symmetry direction in the presence of the reconstruction. The expelled kinks segregate

into regions of 1×1 structure, which must also develop a large step density for the surface to preserve the macroscopic orientation. Thus we can qualitatively predict that the energy saving due to expulsion of the kinks from the 7×7 phase must be greater than the energy cost of forming kinks and steps in the 1×1 phase, as well as the energy cost of the step–step interactions in the 1×1 phase. We can quantify this prediction by using eqs. (10a) and (12) for the special case of $\theta_b = 0$, resulting in a convenient form for the second equality describing this phase separation:

$$\begin{aligned} & \frac{\beta_a(\theta_a, T)}{h_a} \cos \theta_a - \frac{\beta_b(0, T)}{h_b} \\ &= 3g_b(0, T) \tan^2 \phi_b \\ & \quad - 3g_a(\theta_a, T) \tan^2 \phi_a \cos \theta_a \\ & \quad + \left(\frac{1}{h_a} \frac{\partial \beta_a}{\partial \tan \theta} \Big|_{\theta_a} + \frac{\partial g_a}{\partial \tan \theta} \Big|_{\theta_a} \tan^2 \phi_a \right) \\ & \quad \times \frac{\tan \theta_a}{\cos \theta_a}. \end{aligned} \quad (27)$$

Using the values of the angles listed in table 1 and the step interaction terms listed in table 3, and explicitly evaluating the azimuthal derivatives of the 1×1 phase, gives the difference between

Table 3
Energy values for steps near the $[2\bar{1}1]$ azimuth

T (°C)	$g_a(\theta, T)$ (meV/Å ²)	$\Delta f^0(T)$ (meV/Å ²)	$\left[\frac{\partial \beta_a}{\partial \tan \theta} \right]_{\theta_a}$ (meV/Å)	$\left[\frac{\partial g_a}{\partial \tan \theta} \right]_{\theta_a}$ (meV/Å ²)	$\beta_a \cos \theta_a - \frac{1}{3}\beta_b$ (meV/Å)
845	17 ± 5	–	2 ± 1	10 ± 2	–
820	19 ± 5	0.09 ± 0.03	3 ± 1.5	16 ± 3	–1 ^{+0.7} _{–1.5}
800	20 ± 5	0.14 ± 0.04	4 ± 1.5	19 ± 3	–2 ^{+0.1} _{–1.6}
770	21 ± 5	0.30 ± 0.07	3 ± 1.5	25 ± 3	–3 ± 2

The subscript a refers to the high-temperature “ 1×1 ” phase, and the subscript b refers to the low-temperature 7×7 phase. The values $\epsilon = 0.18 \pm 0.02 \text{ eV}$ and $A = 0.15 \pm .05 \text{ eV}/\text{\AA}$ were used in eqs. (24) and (25) to obtain the step-interaction prefactor for the 1×1 phase. These values were used with $g_b(0, T) = 0.007 \pm 0.002 \text{ eV}/\text{\AA}^2$ and the values of the phase boundary from table 1, to obtain the difference in the surface tension $\Delta f^0(T)$ of the 1×1 and 7×7 phases from eq. (14). The values of the slopes of the step energy and the step interaction term in the 1×1 phase were calculated numerically from eqs. (19) and (25). The difference in the step energies in the 1×1 and 7×7 phase was calculated using eq. (27), with the assumption that the height of the step in the 7×7 phase is 3 times that in the 1×1 phase. The uncertainties listed in the table reflect the error bars on the input parameters: the effect of experimental uncertainty in the phase diagram is reflected in the limited number of significant figures in the reported values.

Table 4
Energy values for steps near the $[2\bar{1}\bar{1}]$ azimuth

T (°C)	$\beta_a(\theta, T)$ (meV/Å)	$\beta_b(0, T)$ (meV/Å) (triple-height steps)	$\left[\frac{\partial \beta_b}{\partial \tan \theta} \right]$ (meV/Å) (lower limit)	$\left[\frac{\partial \beta_b}{\partial \tan \theta} \right]$ (meV/Å) (eq. (19))
845	39 ± 7	–	–	93
820	40 ± 7	119 ± 17	52 ± 11	94
800	41 ± 7	119 ± 15	65 ± 12	95
770	42 ± 7	121 ± 14	87 ± 12	98

The subscript a refers to the high-temperature “ 1×1 ” phase, and the subscript b refers to the low-temperature 7×7 phase. The value $\varepsilon \approx 0.18 \pm 0.02$ was used in eq. (19) to obtain the step energy $\beta_a(\theta, T)$ in the 1×1 phase, and thus using the values from tables 1 and 3, the energy of triple-height steps $\beta_b(0, T)$ in the 7×7 phase. The lower limit of the slope of the step energy in the 7×7 phase was calculated using eq. (28) and values from tables 1 and 3. The slope of the step energy was calculated by evaluating eq. (19) with a kink energy of 3.2 eV, and then numerically differentiating the result at $\theta = 0.05^\circ$. The uncertainties listed in the table reflect the error bars on the input parameters: the effect of experimental uncertainty in the phase diagram is reflected in the limited number of significant figures in the reported values.

the step free energies in the two phases of $\beta_a \cos \theta_a - \frac{1}{3}\beta_b$, which is listed in table 3. The result indicates that steps are slightly more favorable in the 7×7 phase than in the 1×1 phase along this azimuth. Consequently, there is no tendency for a large decrease in density of steps in the reconstructed phase during the phase separation. This allows us to understand why the polar angle of the 7×7 phase decreases only slightly during azimuthal phase separation.

It is now possible to estimate the free energy of triple-height steps in the 7×7 phase by calculating the step energy in the 1×1 phase, assuming $\varepsilon_a = 0.18 \pm 0.02$ eV, and adding the result to the difference calculated from eq. (27), as shown in table 4. The result is the same, 120 ± 15 meV/Å, at all three temperatures, indicating internal consistency in the calculation. If we use the result mentioned above, that the energy cost for forming a triple-height step from three-single height steps is negligibly small [63,75,77], we can estimate the cost of a single height step in the 7×7 phase to be $\beta_b^{\text{single}} \approx 40 \pm 5$ meV/Å along the $[2\bar{1}\bar{1}]$ azimuth. In the symmetric model for the

step, we can also estimate the kink energies for both single and triple height steps in the 7×7 phase to be the step energy times the length of the 7×7 unit cell, giving, and $\varepsilon_b^{\text{single}} \approx 1.1 \pm 0.13$ eV, and $\varepsilon_b^{\text{triple}} \approx 3.2 \pm 0.4$ eV. (If we chose to consider the anisotropic Ising model to describe the step energy, with the kinks on steps of this symmetry having the structure of the $[2\bar{1}\bar{1}]$ step edge, then these estimates of the kink energies would increase by about 35%.)

We can check the internal consistency of the kink and step energies estimated in the previous paragraph by using the inequality for this case which can also be obtained using eq. (15). The result is

$$\begin{aligned} & \frac{1}{h_b} \frac{\partial \beta_b}{\partial \tan \theta} \Big|_{\theta_b=0} - \frac{1}{h_a \cos \theta_a} \frac{\partial \beta_a}{\partial \tan \theta} \Big|_{\theta_a} \\ & > \left(\frac{\beta_a}{h_a} + 3g_a \tan^2 \phi_a \right) \sin \theta_a \\ & \quad + \frac{\partial g_a}{\partial \tan \theta} \Big|_{\theta_a} \frac{\tan^2 \phi_a}{\cos \theta_a}. \end{aligned} \quad (28)$$

The lower limit for the slope of the step energy in the 7×7 phase calculated using eq. (28) is listed in table 4. To check the internal consistency of the model, we can compare this value with the slope calculated using the symmetric Ising results, eq. (19), using a kink energy of 3.2 eV. The result, shown in the last column of table 4, is in each case greater than the lower limit, confirming that the simple model proposed is adequate to describe the observations.

4.3. The orientational phase diagram of vicinal Si(111)

In the preceding two sections, we have analyzed the phase boundaries of the two observed faceting transitions. The parameters that we have extracted from this analysis are sufficient to allow us to calculate the reduced surface tension for vicinal Si(111) as a function of both polar and azimuthal angle, and thus the complete orientational phase diagram. A comparison of the calcu-

Table 5
Parameters to describe the complete phase diagram of Si(111)

	ϵ (eV)	A (eV Å)	β (0, 800°C) (meV/Å) (eqs. (9), (19))	g (0, 800°C) (eV/Å ²) (eqs. (9), (25))
7 × 7 phase				
[$\bar{2}11$] azimuth (single-height steps)	> 1.5	0.40	> 55	0.022
[$2\bar{1}\bar{1}$] azimuth (triple height steps)	3.2	3.6	120	0.007
1 × 1 phase				
[$\bar{2}11$] and [$2\bar{1}\bar{1}$] azimuth	0.18	0.15	40	0.014

The parameters needed to describe the complete phase diagram of Si(111) within a nearest-neighbor square lattice model with elastic step-step interactions are the kink energies ϵ and the step-step interaction strength A in the high- (7×7) and low- (1×1) temperature phases, and the temperature variation of the difference in the surface tension $\Delta f^0(T)$ of the two phases on the singular (perfectly oriented) (111) surface. Near the transition we have calculated the rate of variation of the difference in surface tension $\Delta f^0(T) \Delta T$ with temperature to be $3.5 \times 10^{-6} \text{ eV/Å}^2 \cdot \text{K}$, as shown in tables 2 and 3. The values for the kink energies and the step interaction energies deduced from experimental observations are listed in the table. Representative values of the step energies $\beta(0, T)$ and the contribution of the step interactions $g(0, T)$ along the two high symmetry directions calculated using these values are listed in the next two columns. For the 7×7 phase, the kink energies are large enough that thermal excitations at the transition temperature are negligible, and the step and interaction terms are independent of temperature. For the 1×1 phase, the temperature dependence of these terms is small but not zero, as listed in table 2.

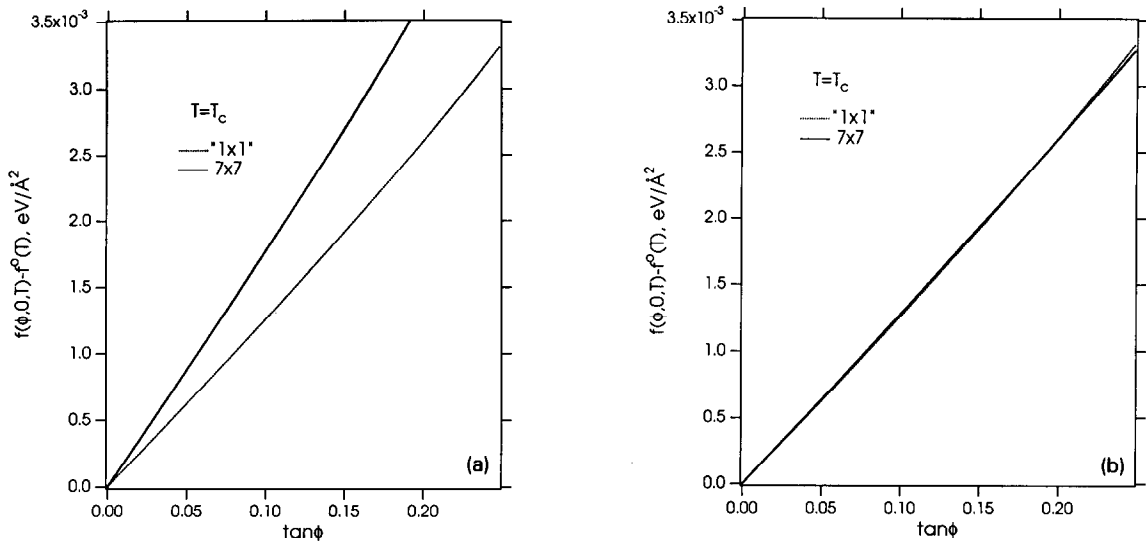


Fig. 10. Intersecting reduced surface tension curves, calculated with the parameters of table 5, at the temperature of the 7×7 and " 1×1 " phase transition on the (111) facet, $T_c = 845^\circ\text{C}$. As the temperature decreases, the difference in surface tension on the facet, $\Delta f^0(T)$, between the two phases changes, causing the two curves to sweep through each other. The nature of the intersection of the two curves determines the orientational phase diagram. The rate of change of $\Delta f^0(T)$ with temperature was determined by fitting the experimental data to be $3.5 \times 10^{-6} \text{ eV/Å}^2 \cdot \text{K}$. (a) The two reduced surface tension curves calculated for a surface misoriented along the high-symmetry [$\bar{2}11$] direction. The intersection of the curves leads to faceting. The transition temperature is depressed with increasing angle, such that the (simultaneous) appearance of the 7×7 reconstruction and the faceting appears about 60°C below T_c for surfaces with step density of 0.2 (miscut angle about 11°). (b) The two reduced surface tension curves calculated for a surface misoriented along the high symmetry [$2\bar{1}\bar{1}$] direction. The two curves overlap almost perfectly at the transition, with the result that the transition occurs within a temperature range of less than $\pm 5^\circ\text{C}$ over the entire range of step densities shown (corresponding to a miscut of up to 14°).

lated phase diagram with the experimental observations of fig. 2 is the final consistency check on the results of the analysis above. The parameters that will be used for this final check, as well as some representative values of the terms in the expression of eq. (9) for the reduced surface tension are listed in table 5. To calculate the orientational phase diagram, we first calculate the reduced surface tension curves for the 7×7 and 1×1 phases, and then use eqs. (10)–(14) to evaluate the positions of the tie-bars. The first step in this process, calculation of the reduced surface tension, is illustrated in fig. 10. The reduced surface tension curves at 845°C , the transition temperature on the (111) facet, are shown in fig. 10 for the two high symmetry orientations of the surface. For the $[\bar{2}11]$ direction, the variation of the reduced surface tension with step density is distinctly different for the high- and low-temperature phases. As the relative surface tension of the two phases on the facet ($\phi = 0$) changes with temperature, the intersection of the two curves moves to larger and larger values of the polar angle ϕ , leading to the faceting which is observed experimentally. In contrast, in the $[2\bar{1}\bar{1}]$ direction the reduced surface tension curves of the two phases are very similar in shape. As a result, the

two curves cross completely within $\pm 5^\circ\text{C}$ of the transition temperature. Thus, along this azimuth, the calculated reconstructive transition temperature is independent of the macroscopic polar angle ϕ_0 , and the surface is orientationally stable as observed experimentally. The calculated full two-dimensional phase diagram is shown in fig. 11. The calculation reproduces quantitatively all the experimental observations. In particular, two initially puzzling experimental observations, the angle-independent phase transition temperature along the $[2\bar{1}\bar{1}]$ azimuth, and the temperature-independent polar angle in the azimuthal phase separation, are predicted naturally within the simple model chosen to describe the surface.

4.4. Physical interpretation of the energetic parameters

It is clear from figs. 10 and 11 that the model used, a square nearest-neighbor lattice with step-step interactions, can reproduce quantitatively all of our experimental observations. Given the simplicity of this model, it is not obvious how accurately the energetic parameters calculated represent the true energies of the surface. To address this issue, we consider how the energy

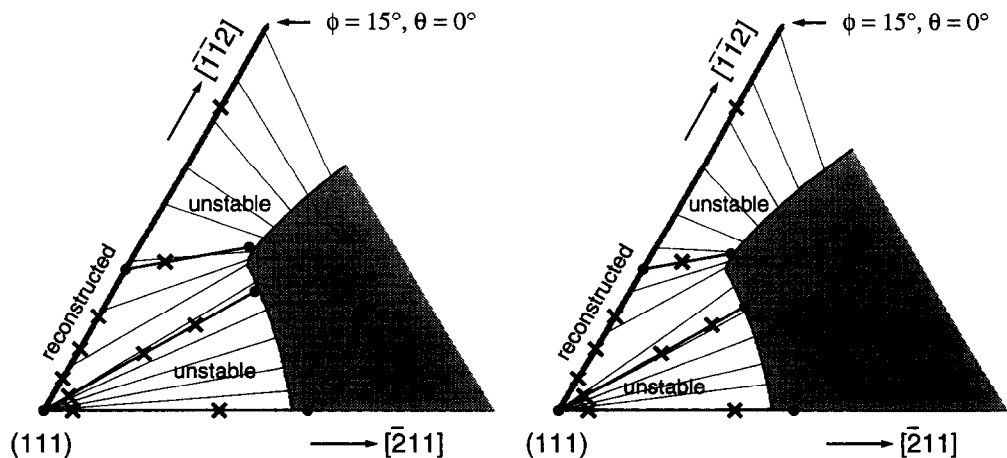


Fig. 11. Calculated orientation phase diagrams of vicinal Si at 800°C (using $\Delta f^0(T) = 0.13 \text{ meV}/\text{\AA}^2$) and 820°C (using $\Delta f^0(T) = 0.08 \text{ meV}/\text{\AA}^2$), showing the form of the tie lines at various positions in density space. (Following eq. (8), this diagram is a polar plot of $\tan \phi$.) The tie-bars indicate phase separation between orientations of the high-temperature “ 1×1 ” structure, which exists in the shaded regions, and the low-temperature 7×7 structure which is stable along the $[2\bar{1}\bar{1}]$ axis and on the (111) surface. The \times 's and the heavy tie-bars show the experimental observations (also shown in fig. 2).

scale is set within our model. The three energies which we put into the model initially are the step–step interaction energies in the two phases and the kink energy in the high-temperature phase. The determination of the step–step interaction energies is independent of any of the assumptions of the statistical model used to describe the step structure; thus the parameters that are determined primarily by the step interactions will be the least affected by the details of the lattice model. These parameters are the difference between the surface tension of the two phases (eqs. (14) and (17)), and the difference between the step energies in the two phases (eq. (26) and column 4 in table 2, and eq. (27) and column 5 in table 3). In contrast, the choice of the kink energy (0.18 eV) which we used for the high temperature phase is strongly influenced by the lattice model under consideration. Within the square-lattice model, the value chosen is the highest energy consistent with both the observation of a symmetric shape for two-dimensional pits. However, if we allowed anisotropy in the model, or if we chose a different lattice symmetry, such as a honeycomb lattice [80,81], then larger values of the kink energy would be consistent with the observations, including the measured value of the step stiffness [60]. (A larger value of the kink energy would also be more

consistent with Chadi's estimates of step energies [79].) Thus our calculated values which depend on the absolute value of the kink energy in the high temperature phase are model dependent, and may be quite different from their physical counterparts. The quantities in particular for which this is true are the absolute values of the step energies in both phases, and the step energy in the high temperature phase. The dependence of the calculated values on model symmetry and on the value of the kink energy is illustrated in table 6. The results show that changing the kink energy by a factor of two, and changing from square to rectangular symmetry affects the calculated differences in surface tension and step energy only slightly. In contrast, the absolute values of the step energies scale roughly linearly with the kink energy.

In summary, since we find that the simplest description of the steps is adequate to reproduce the thermodynamic observations, we cannot expect to be able to use such observations to deduce information about the appropriate statistical mechanical Hamiltonian. Furthermore, the thermodynamic observations are not sufficient to set the absolute energy scale. Independent observations of step–step interaction energies are needed to obtain believable estimates of the differences in energies between the two phases. To deter-

Table 6

Illustration of the effect of model symmetry, and changes in the energy scale through the value of the kink energy ϵ in the 1×1 phase

ϵ (eV) (1×1 phase)	$\beta_a(0, 0)$ (meV/Å) (1×1 phase)	Δf^0 (645°C) (meV/Å ²)	$\beta_b(0, 0) - \beta_a(0, 0)$ (meV/Å) (single-height steps)		$\beta_b(0, 0)$ (meV/Å) (single-height)	$\beta_b(0, 0)$ (meV/Å) (triple-height)
			$[\bar{2}11]$	$[2\bar{1}\bar{1}]$		
			azimuth	azimuth		
0.18	47	0.8	> 12	–7	> 55	120
0.36	94	0.6	> 9	–7	> 101	260
0.18	94	0.8	> 12	–7	> 106	260
0.36	188	0.6	> 9	–5	> 197	544
0.18	23	0.8	> 12	–6	> 35	53

The first two rows show values for a square-lattice model of the step edge, i.e. with $\epsilon/a_p = \beta(0, 0)$. The next two rows show values for a rectangular lattice model with $\epsilon/a_p = 0.5\beta(0, 0)$. The last row shows values for a rectangular lattice model with $\epsilon/a_p = 2\beta(0, 0)$. Differences in the surface tension and differences in the step energy are changed little by changes in the symmetry or absolute energy scale. The calculated absolute values of the step energies $\beta_b(0, 0)$ in the low-temperature (7×7) phase scale roughly linearly with the value used for $\beta_a(0, 0)$.

mine accurate absolute values of step energies from an analysis of the experimental observations, one also needs to have independent information on the symmetry and energy scale of the system. For Si(111), the accuracy of the values determined from the analysis of the observed phase diagrams could be increased dramatically given an accurate value of the kink energy and structure in the relatively simple “ 1×1 ” phase.

5. Conclusions

We have described in detail the thermodynamic formalism of orientational phase separation induced by a first-order change on the low-index surface, and shown how orientational stability can be understood in terms of microscopic energetic parameters of the surface. A particularly important, and general, point which derives from this presentation is the role of step–step interactions in setting the energy scale of the problem. As shown in eqs. (14) and (17), a process which changes the surface tension by amounts comparable to the step-interaction term in the free energy is required to induce an orientational instability. It is reasonable to assume that on most surfaces the magnitude of the step interactions will be comparable to the stress-mediated interactions on Si(111) [82]. Thus using eq. (25), we find that processes which change the surface tension by amounts on the order of only one $\text{meV}/\text{\AA}^2$, which is easily accomplished by either adsorption or reconstruction, are necessary to induce faceting. To obtain a sufficient condition for faceting, there must also be changes of comparable magnitude in either the step or kink energy [83] to satisfy eqs. (10).

As a specific example, a quantitative and sufficient condition for phase separation between a facet and a step bunch to occur is obtained by combining eqs. (17) and (26). In physical terms, the result is that if the perturbing process affects the surface tension of a facet and the energy cost of steps with opposite signs, it will lead to step bunching. (E.g. if the perturbation simultaneously decreases (increases) the surface tension of a facet and increases (decreases) the energy cost of

steps, it will lead to step bunching with the perturbation concentrated on the facet (step bunch).) Thus given rather qualitative information about how a process (such as adsorption, reconstruction or deposition) affects facet, step and kink energies, it is generally possible to predict whether or not the process will cause faceting.

Using the thermodynamic and statistical mechanical formalism described in sections 2 and 3, we have illustrated, with the specific example of vicinal surfaces of Si(111), how to analyze observations of phase separation to extract information about the surface energetics. This process is generally applicable. One must be aware, however, that given only the phase diagrams, the energetic values determined are specific to the model and may not represent physical energies. However, if additional information is known independently, then accurate determination of the physical energies is possible. It should increasingly be reasonable to expect that good estimates of step interaction energies will be available, determined either from experimental determination of stress [84–87], or from theoretical calculation of stress [74,88], or from direct measurement of step distributions [30,50,53,60,89–91]. With this information one can find good estimates of the change in facet surface tension, and of the differences in step/kink energies between the two phases from the observations of the phase separation. If, in addition, one has a good measurement [47] or calculation of the kink energy and symmetry in one phase [92], then it will be possible to make an accurate determination of the overall variation in surface tension with orientation for both phases.

For our specific example of Si(111), we are able to obtain physically meaningful estimates of the differences in free energy between the 7×7 and “ 1×1 ” phase as a function of temperature, and for the differences in energy between the steps in the two phases. However, as we do not have an unambiguous determination of the kink energy/structure in the high temperature phase to set the absolute energy scale of our calculations, the specific numbers calculated for the step and kink energies are model dependent. Approximating the steps on the surface within the simplest possible model, a square near-neighbor lat-

tice, allows us to determine the internally consistent (but model-dependent) energies listed in table 5. The values which we have determined for the step energies are particularly interesting: for the high- T “ 1×1 ” structure we obtain $\beta(0, 0) = 47 \pm 5$ meV/Å for both of the high symmetry directions; for single height steps on the 7×7 reconstructed surface, $\beta(0, 0) > 55 \pm 8$ meV/Å for the $[\bar{2}11]$ orientation, and $\beta(0, 0) = 40 \pm 5$ meV/Å for the $[2\bar{1}\bar{1}]$ orientation. We can put these values in context of other measurements and calculations of the energetics of Si surfaces. From Chadi’s estimates [79], the difference in step energies (without consideration of the 7×7 reconstruction) in the two directions should be approximately 160 meV/Å, substantially above our lower limit of 15 meV/Å. Our relative values are consistent with the experimental result that the step energy anisotropy is 1.2–1.25 [59]. Our values are also consistent with a recent estimate of the step energy of approximately 40 meV/Å based on a direct observation of the Si crystal shape [93]. Our values are substantially lower than calculated values of 260 meV/Å for the $[\bar{2}11]$ steps, and 140 meV/Å for the $[2\bar{1}\bar{1}]$ steps, which were obtained using an empirical potential with a 1×1 structure for the surface [94]. As would be expected based on bond counting arguments, the step energies for Si(111) are substantially higher than the values of 3–7 and 23–39 meV/Å for the two types of steps on Si(100) [47,95]. The physical significance of the magnitude of the step energies can be seen by comparing the step energies to the surface tension. The ratio of $(\beta/h)/f^0$ is equal to the ratio of the facet width to the crystal radius [36]. The surface energy of Si(111) is approximately 90 meV/Å² [96–98]. Using the values for the step energies above, we find that the width-to-radius ratio of the (111) facet will be greater than 0.14. This value is surprisingly small from bond-counting determinations of the equilibrium crystal shape which give a ratio of $1/\sqrt{2}$ [99] and somewhat smaller than observed in the shape of small cavities in Si [93,100]. However, it is consistent with observations of a large range of stable surface orientations for Si [101,102] which suggest a smooth crystal shape. By combining our observa-

tions with information based on semi-empirical [103] and first principles calculations [97,98,104] of the energies of Si surfaces, it is reasonable to expect that a quantitative, predictive understanding of Si morphology will soon be a reality.

Acknowledgements

This work has been supported by the ONR (E.D.W. and J.W.), the NSF-MRG (N.C.B. and T.L.E.) and the DOD (R.J.P.). We are also grateful to Dr. Y. Yang for constructive suggestions on several drafts of this manuscript.

Appendix

In deriving eqs. (10)–(17), we wish to begin with a thermodynamic function, the reduced surface tension f , expressed in terms of thermodynamic step and kink densities $\tan \phi$ and $\tan \theta$, and take its partial derivatives along two orthogonal directions, on which both θ and ϕ are varying. The geometry of interest is illustrated in fig. 12. We evaluate the derivatives by first writing the differential off in terms of $\rho = \tan \phi$ and $\eta = \tan \theta$:

$$df = \left. \frac{\partial f}{\partial \rho} \right|_{\eta} d\rho + \left. \frac{\partial f}{\partial \eta} \right|_{\rho} d\eta. \quad (\text{A.1})$$

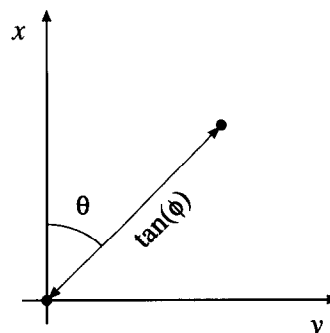


Fig. 12. Coordinate transform. Illustration of the relationship between the x – y and the θ – ϕ coordinate systems.

We can evaluate the partial derivatives with respect to x and y , giving

$$\left. \frac{\partial f}{\partial x} \right|_y = \left. \frac{\partial f}{\partial \rho} \right|_{\eta} \left. \frac{\partial \rho}{\partial x} \right|_y + \left. \frac{\partial f}{\partial \eta} \right|_{\rho} \left. \frac{\partial \eta}{\partial x} \right|_y, \quad (\text{A.2a})$$

and

$$\left. \frac{\partial f}{\partial y} \right|_x = \left. \frac{\partial f}{\partial \rho} \right|_{\eta} \left. \frac{\partial \rho}{\partial y} \right|_x + \left. \frac{\partial f}{\partial \eta} \right|_{\rho} \left. \frac{\partial \eta}{\partial y} \right|_x. \quad (\text{A.2b})$$

The partial derivatives of ρ and η with respect to x and y can be evaluated using the geometrical relationships:

$$x = \tan \phi \cos \theta, \quad (\text{A.3a})$$

$$y = \tan \phi \sin \theta, \quad (\text{A.3b})$$

$$\tan \theta = y/x, \quad (\text{A.3c})$$

$$x^2 + y^2 = \tan^2 \phi. \quad (\text{A.3d})$$

The resulting forms for the partial derivatives of f are:

$$\left. \frac{\partial f}{\partial x} \right|_y = \left. \frac{\partial f}{\partial \rho} \right|_{\eta} \cos \theta + \left. \frac{\partial f}{\partial \eta} \right|_{\rho} \left(\frac{-\tan \theta}{\tan \phi \cos \theta} \right) \quad (\text{A.4a})$$

and

$$\left. \frac{\partial f}{\partial y} \right|_x = \left. \frac{\partial f}{\partial \rho} \right|_{\eta} \sin \theta + \left. \frac{\partial f}{\partial \eta} \right|_{\rho} \left(\frac{1}{\tan \phi \cos \theta} \right), \quad (\text{A.4b})$$

which lead directly to eqs. (12) and (13) with the substitution $\rho_x = x$ and $\rho_y = y$.

References

- [1] G. Ertl, *Science* 254 (1991) 1750.
- [2] M.G. Lagally, Ed., *Kinetics of Ordering and Growth at Surfaces* (Plenum, New York, 1990).
- [3] A.J.W. Moore, in: *Metal Surfaces*, Eds. W.D. Robertson and N.A. Gjostein, (American Society of Metals, Metals Park, Ohio, 1962) p. 155.
- [4] J.C. Tracy and J.M. Blakely, *Surf. Sci.* 13 (1968) 313.
- [5] M. Flytzani-Stephanopoulos and L.D. Schmidt, *Prog. Surf. Sci.* 9 (1979) 83.
- [6] E. Suliga and M. Henzler, *Jpn. J. Appl. Phys.* 16 (1983) 1543.
- [7] E.D. Williams and N.C. Bartelt, *Ultramicroscopy* 31 (1989) 36.
- [8] J. Falta, R. Imbihl and M. Henzler, *Phys. Rev. Lett.* 64 (1990) 1409.
- [9] J. Falta, R. Imbihl, M. Sander and M. Henzler, *Phys. Rev. B* 45 (1992) 6568.
- [10] T.E. Madey, J. Guan, C.-Z. Dong and S.M. Shivaprasad, *Surf. Sci.* 287/288 (1993) 826.
- [11] C. Herring, *Phys. Rev.* 82 (1951) 87.
- [12] One should note that kinetic mechanisms can give rise to a faceted surface, so the first question in any experimental observation must be whether or not the faceted surface represents an equilibrium structure.
- [13] M. Drechsler, *Surf. Sci.* 162 (1985) 755.
- [14] R.J. Phaneuf and E.D. Williams, *Phys. Rev. Lett.* 58 (1987) 2563.
- [15] R.J. Phaneuf, E.D. Williams and N.C. Bartelt, *Phys. Rev. B* 38 (1988) 1984.
- [16] J.C. Heyraud, J.J. Métois and J.M. Bermond, *J. Cryst. Growth* 98 (1989) 355.
- [17] J. Wei, X.-S. Wang, N.C. Bartelt, E.D. Williams and R.T. Tung, *J. Chem. Phys.* 94 (1991) 8384.
- [18] M. Dreschler, *Surf. Sci.* 266 (1992) 1.
- [19] H.M. van Pinxteren and J.W.N. Frenken, *Surf. Sci.* 275 (1992) 383.
- [20] B. Binnig and H. Rohrer, *Rev. Mod. Phys.* 59 (1987) 615.
- [21] E. Bauer, *Ultramicroscopy* 17 (1985) 51.
- [22] N. Osakabe, Y. Tanishiro and K. Yagi, *Surf. Sci.* 109 (1981) 353.
- [23] N.C. Bartelt, J.L. Goldberg, T.L. Einstein and E.D. Williams, *Surf. Sci.* 273 (1992) 252.
- [24] N.C. Bartelt, E.D. Williams, R.J. Phaneuf, Y. Yang and S. Das Sarma, *J. Vac. Sci. Technol. A* 7 (1989) 1898.
- [25] J.L. Goldberg, X.-S. Wang, J. Wei, N.C. Bartelt and E.D. Williams, *J. Vac. Sci. Technol. A* 9 (1991) 1868.
- [26] J.L. Goldberg, X.-S. Wang, N.C. Bartelt and E.D. Williams, *Surf. Sci. Lett.* 249 (1991) L285.
- [27] R.Q. Hwang, E.D. Williams and R.L. Park, *Phys. Rev. B* 40 (1989) 11716.
- [28] R.J. Phaneuf and E.D. Williams, *Phys. Rev. B* 41 (1990) 2991.
- [29] R.J. Phaneuf, N.C. Bartelt, E.D. Williams, W. Świąch and E. Bauer, *Phys. Rev. Lett.* 21 (1991) 2986.
- [30] X.-S. Wang, J.L. Goldberg, N.C. Bartelt, T.L. Einstein and E.D. Williams, *Phys. Rev. Lett.* 65 (1990) 2430.
- [31] E.D. Williams and N.C. Bartelt, *Science* 251 (1991) 393.
- [32] B. Li, N.C. Bartelt and E.D. Williams, in preparation.
- [33] J.W. Gibbs, in: *The Scientific Papers of J. Willard Gibbs* (Dover, New York, 1961).
- [34] R. Kern, in: *Morphology of Crystals*, I. Sunagawa, Eds. (Terra Scientific Publishing Co., Tokyo, 1987) p. 79.
- [35] C. Jayaprakash, C. Rottman and W.F. Saam, *Phys. Rev. B* 39 (1984) 6549.
- [36] M. Wortis, in: *Chemistry and Physics of Solid Surfaces*, Vol. 7, Eds. R. Vanselow and R.F. Howe (Springer, Berlin, 1988) p. 367.
- [37] C. Rottman and M. Wortis, *Phys. Rep.* 124B (1984) 241.
- [38] N.C. Bartelt, T.L. Einstein and C. Rottman, *Phys. Rev. Lett.* 66 (1991) 961.

- [39] A.A. Chernov, *Sov. Phys. Usp.* 4 (1961) 1116.
- [40] J.E. Métois and J.C. Heyraud, *Ultramicroscopy* 31 (1989) 73.
- [41] H.M. van Pinxteren and J.W.M. Frenken, *Europhys. Lett.* 21 (1993) 43.
- [42] N.C. Bartelt, in preparation.
- [43] N.C. Bartelt, T.L. Einstein and E.D. Williams, *Surf. Sci.* 276 (1992) 308.
- [44] G.A. Somorjai and M.A. Van Hove, *Prog. Surf. Sci.* 30 (1989) 201.
- [45] J.W. Cahn, *J. Phys. (Paris) C6* 43 (1982) 199.
- [46] P. Nozières, in: *Solids Far From Equilibrium*, Ed. C. Godrèche (Cambridge University Press, Cambridge, 1991) p. 1.
- [47] B.S. Swartzentruber, Y.-W. Mo, R. Kariotis, M.G. Lagally and M.B. Webb, *Phys. Rev. Lett.* 65 (1990) 1913.
- [48] Z. Zhang, Y.-T. Lu and H. Metiu, *Surf. Sci. Lett.* 259 (1991) L719.
- [49] B. Joós, T.L. Einstein and N.C. Bartelt, *Phys. Rev. B* 43 (1991) 8153.
- [50] J. Frohn, M. Giesen, M. Poensgen, J.F. Wolf and H. Ibach, *Phys. Rev. Lett.* 67 (1991) 3543.
- [51] A.C. Redfield and A. Zangwill, *Phys. Rev. B* 46 (1992) 4289.
- [52] C. Rottman and M. Wortis, *Phys. Rev. B* 24 (1981) 6274.
- [53] D. Dijkkamp, A.J. Hoeven, E.J. van Loenen, J.M. Lenssen and J. Dieleman, *Appl. Phys. Lett.* 56 (1990) 39.
- [54] J.E. Avron, H. van Beijeren, L.S. Schulman and R.K.P. Zia, *J. Phys. A* 15 (1982) L81.
- [55] M.E. Fisher, *J. Stat. Phys.* 34 (1984) 667.
- [56] M.E. Fisher and D.S. Fisher, *Phys. Rev. B* 25 (1982) 3192.
- [57] B. Sutherland, *Phys. Rev. A* 4 (1971) 1971.
- [58] R.J. Phaneuf and E.D. Williams, *Phys. Rev. B* 35 (1987) 4155.
- [59] K. Yagi, A. Yamana, H. Sato, M. Shima, H. Ohse, S. Ozawa and Y. Tanishiro, *Prog. Theor. Phys. Suppl.* 106 (1991) 303.
- [60] C. Alfonso, J.M. Bermond, J.C. Heyraud and J.J. Métois, *Surf. Sci.* 262 (1992) 371.
- [61] In making this analysis we have assumed a kink separation of 3.84 Å, and a kink depth of 3.33 Å. We have also assumed that the measured step-edge stiffness corresponds to the high symmetry direction, $\theta = 0$, which gives us the minimum value for the kink energy. The calculated value of the kink energy could increase by nearly a factor of two within this model if the analysis assumed larger azimuthal angles.
- [62] N.C. Bartelt, T.L. Einstein and E.D. Williams, *Surf. Sci. Lett.* 240 (1991) L591.
- [63] E.D. Williams and N.C. Bartelt, *Proc. Conf. on Surf. Disorder, Les Houches, 1992*, to be published.
- [64] W. Teliens and E. Bauer, *Ber. Bunsenges. Phys. Chem.* 90 (1986) 197.
- [65] U. Kohler, J.E. Demuth and R.J. Hamers, *J. Vac. Sci. Technol. A* 7 (1989) 2860.
- [66] E.D. Williams, R.J. Phaneuf, N.C. Bartelt, W. Świąch and E. Bauer, *Mat. Res. Soc. Symp. Proc.* 238 (1992) 219.
- [67] S.-I. Kitamura, T. Sato and M. Iwatsuki, *Nature* 351 (1991) 215.
- [68] D.Y. Noh, K.I. Blum, M.J. Ramstad and R.J. Birge-neau, *Phys. Rev. B* 44 (1991) 10969.
- [69] H. Hibino, Y. Shinoda, Y. Kobayashi and K. Sugii, *Jpn. J. Appl. Phys.* 30 (1991) 1337.
- [70] B.S. Swartzentruber, Y.-W. Mo, M.B. Webb and M.G. Lagally, *J. Vac. Sci. Technol. A* 7 (1989) 2901.
- [71] R. Wiesendanger, G. Tarrach, D. Burgler and H.-J. Güntherodt, *Europhys. Lett.* 12 (1990) 57.
- [72] D. Rogers and T. Tiedje, *Surf. Sci. Lett.* 274 (1992) L599.
- [73] H. Hibino, T. Fukuda, M. Suzuki, Y. Homma, T. Sato, M. Iwatsuki, M. Miki and H. Tokumoto, *Phys. Rev. B* 47 (1993) 13027.
- [74] R.D. Meade and D. Vanderbilt, *Phys. Rev. Lett.* 63 (1989) 1404.
- [75] J. Wei, X.-S. Wang, N.C. Bartelt and E.D. Williams, in preparation.
- [76] V.I. Mashanov and B.X. Ol'shanetskii, *JETP Lett.* 36 (1982) 355.
- [77] J. Wei, X.-S. Wang, J.L. Goldberg, N.C. Bartelt and E.D. Williams, *Phys. Rev. Lett.* 69 (1992) 3885.
- [78] The uncertainty on the kink energy is used to illustrate the effect of statistical uncertainty on the calculation of other parameters; there is a serious systematic uncertainty in this value which is not represented in this error bar.
- [79] D.J. Chadi and J.R. Chelikowsky, *Phys. Rev. B* 24 (1981) 4892.
- [80] E.E. Gruber and W.W. Mullins, *J. Phys. Chem. Solids* 28 (1967) 875.
- [81] R.K.P. Zia, *J. Stat. Phys.* 45 (1986) 801.
- [82] D. Wolf and J.A. Jaszczak, *Surf. Sci.* 277 (1992) 301.
- [83] In comparing magnitudes of surface, step and kink energies, it is necessary to normalize all to an energy per unit area, e.g. divide the step energy by step height, and divide the kink energy by kink height and kink length.
- [84] M.B. Webb, F.K. Men, B.S. Swartzentruber and M.G. Lagally, *J. Vac. Sci. Technol. A* 8 (1990) 2658.
- [85] R.E. Martinez, W.M. Augustyniak and J.A. Golovchenko, *Phys. Rev. Lett.* 64 (1990) 1035.
- [86] D. Sander, U. Linke and H. Ibach, *Surf. Sci.* 272 (1992) 318.
- [87] D. Sander and H. Ibach, *Phys. Rev. B* 43 (1992) 4263.
- [88] M. Mansfield and R.J. Needs, *Phys. Rev. B* 43 (1991) 8829.
- [89] G.P. Kochanski, *Phys. Rev. B* 41 (1990) 12334.
- [90] M.B. Webb, F.K. Men, B.S. Swartzentruber, R. Kariotis and M.G. Lagally, *Surf. Sci.* 242 (1991) 23.
- [91] S. Rousset, S. Gauthier, O. Siboulet, J.C. Girard, S. de Cheveigne, M. Huerta-Garnica, W. Sacks, M. Belin and J. Klein, *Ultramicroscopy* 42-44 (1992) 515.

- [92] R.C. Nelson, T.L. Einstein, S.V. Khare and P.J. Rous, *Surf. Sci.*, in press.
- [93] D.J. Eaglesham, A.E. White, L.C. Feldman, N. Moriya and D.C. Jacobson, *Phys. Rev. Lett.* 70 (1993) 1643.
- [94] E. Pearson, T. Takai, T. Halicioglu and W.A. Tiller, *J. Cryst. Growth* 70 (1984) 33.
- [95] D.J. Chadi, *Phys. Rev. Lett.* 59 (1987) 1691.
- [96] R.D. Meade and D. Vanderbilt, *Phys. Rev.* 40 (1989) 3905.
- [97] K.D. Brommer, M. Needels, B.E. Larson and J.D. Joannopoulos, *Phys. Rev. Lett.* 68 (1992) 1355.
- [98] I. Stich, M.C. Payne, R.D. King-Smith, J.-S. Lin and L.J. Clarke, *Phys. Rev. Lett.* 68 (1992) 1351.
- [99] G.A. Wolff and J.G. Gualtieri, *Am. Mineral.* 47 (1962) 562.
- [100] D.M. Follstaedt, *Appl. Phys. Lett.* 62 (1993) 1116.
- [101] B.Z. Olshanetsky and A.A. Shklyaev, *Surf. Sci.* 82 (1979) 445.
- [102] B.Z. Olshanetsky and V.I. Mashanov, *Surf. Sci.* 111 (1981) 414.
- [103] S. Das Sarma and K.E. Khor, *Appl. Surf. Sci.* 60/61 (1992) 99.
- [104] D.M. Bird, L.J. Clarke, R.D. King-Smith, M.C. Payne, I. Stich and A.P. Sutton, *Phys. Rev. Lett.* 69 (1992) 3785.